Review of Scientific Instruments

A low-temperature scanning probe microscopy system with molecular beam epitaxy and optical access

Cite as: Rev. Sci. Instrum. **89**, 113705 (2018); https://doi.org/10.1063/1.5046466
Submitted: 28 June 2018 • Accepted: 18 October 2018 • Published Online: 08 November 2018

Ze-Bin Wu, Zhao-Yan Gao, Xi-Ya Chen, et al.

AIP Publishing

REVIEW OF SCIENTIFIC INSTRUMENTS **89**, 113705 (2018)

A low-temperature scanning probe microscopy system with molecular beam epitaxy and optical access

Ze-Bin Wu,[1,2,a)] Zhao-Yan Gao,[1,2,a)] Xi-Ya Chen,[1,2] Yu-Qing Xing,[1,2] Huan Yang,[1,2] Geng Li,[1] Ruisong Ma,[1] Aiwei Wang,[1,2] Jiahao Yan,[1,2] Chengmin Shen,[1] Shixuan Du,[1,3,4] Qing Huan,[1,3,4,b)] and Hong-Jun Gao[1,2,3,4,b)]

[1]*Beijing National Laboratory for Condensed Matter Physics and Institute of Physics, Chinese Academy of Sciences, Beijing 100190, China*
[2]*School of Physical Sciences, University of Chinese Academy of Sciences, Beijing 100190, China*
[3]*CAS Center for Excellence in Topological Quantum Computation, University of Chinese Academy of Sciences, Beijing 100190, China*
[4]*Songshan Lake Materials Laboratory, Dongguan, Guangdong 523808, China*

(Received 28 June 2018; accepted 18 October 2018; published online 8 November 2018)

A low-temperature ultra-high vacuum scanning probe microscopy (SPM) system with molecular beam epitaxy (MBE) capability and optical access was conceived, built, and tested in our lab. The design of the whole system is discussed here, with special emphasis on some critical parts. The SPM scanner head takes a modified Pan-type design with improved rigidity and compatible configuration to optical access and can accommodate both scanning tunneling microscope (STM) tips and tuning-fork based qPlus sensors. In the system, the scanner head is enclosed by a double-layer cold room under a bath type cryostat. Two piezo-actuated focus-lens stages are mounted on both sides of the cold room to couple light in and out. The optical design ensures the system's forward compatibility to the development of photo-assisted STM techniques. To test the system's performance, we conducted STM and spectroscopy studies. The herringbone reconstruction and atomic structure of an Au(111) surface were clearly resolved. The *dI*/*dV* spectra of an Au(111) surface were obtained at 5 K. In addition, a periodic 2D tellurium (Te) structure was grown on the Au(111) surface using MBE and the atomic structure is clearly resolved by using STM. *Published by AIP Publishing.* https://doi.org/10.1063/1.5046466

I. INTRODUCTION

Since the invention of the first scanning tunneling microscope[1] (STM) and the first atomic force microscope[2] (AFM) in 1980s, many different types of scanning probe microscopy (SPM) techniques have been developed. SPM[3,4] is well known for its outstanding spatial resolution on flat material surfaces. On the other hand, molecular beam epitaxy (MBE)[5,6] is a widely used technique for the growth of atomically flat single crystal thin films with high-precision control. The combination of SPM and MBE enables the growth and *in situ* characterization of thin films or low-dimensional materials in a single system[7] and, therefore, has become a widely adopted assembly in many SPM laboratories. For example, many novel 2D materials, such as germanene,[8] $PtSe_2$,[9] CuSe,[10] $MoSe_2$,[11] and $PdTe_2$,[12] and heterostructures, such as $HfTe_3$/$HfTe_5$/Hf[13] and $MoSe_2$/$HfSe_2$,[13,14] have been grown by MBE and then investigated *in situ* by SPM.

The introduction of light into STM can further extend its capability and broaden its applications. For example, the ultrafast STM techniques, such as the femtosecond-laser-coupled STM and the terahertz STM,[15–17] extend the applications of STM to ultrafast studies on electronic excitation behaviors of nanoscale materials and structures. Besides that, there are other cutting-edge techniques that can be developed in a STM system with optical access, such as tip-enhanced Raman spectroscopy (TERS),[18–22] tip-induced photoluminescence,[23] and so on.[24–26]

In this paper, we report the construction and the performance testing of a newly developed low-temperature (LT) SPM system with MBE and two optical access paths. This system is featured by the combination of different techniques in a single system and the forward compatibility to photo-assisted STM research. The homemade SPM scanner head takes a modular design with a unibody titanium frame, and the tip holder accommodates both STM tips and tuning-fork based qPlus sensors. A double-layer cold room is mounted at the bottom of the cryostat, with two piezo-driven focus lenses mounted on both sides. The light path and optical structures inside the vacuum are described in the context. The vacuum level in the SPM chamber and the MBE chamber reaches below 5×10^{-11} Torr after baking. The sample temperature is around 5 K after cooling down. The performance of the STM and MBE is demonstrated by the growth and characterization of a 2D tellurium structure. The system exhibits good stability on STM imaging and is compatible to the introduction of light and thus is expected to be a versatile tool for the growth and the characterization of thin films and low-dimensional materials.

II. SYSTEM DESIGN

A. Whole structure

Figures 1(a) and 1(b) show a 3D model and a photograph of the system. The whole system is fixed on a frame of

a)Z.-B. Wu and Z.-Y. Gao contributed equally to this work.
b)Authors to whom correspondence should be addressed: huanq@iphy.ac.cn and hjgao@iphy.ac.cn

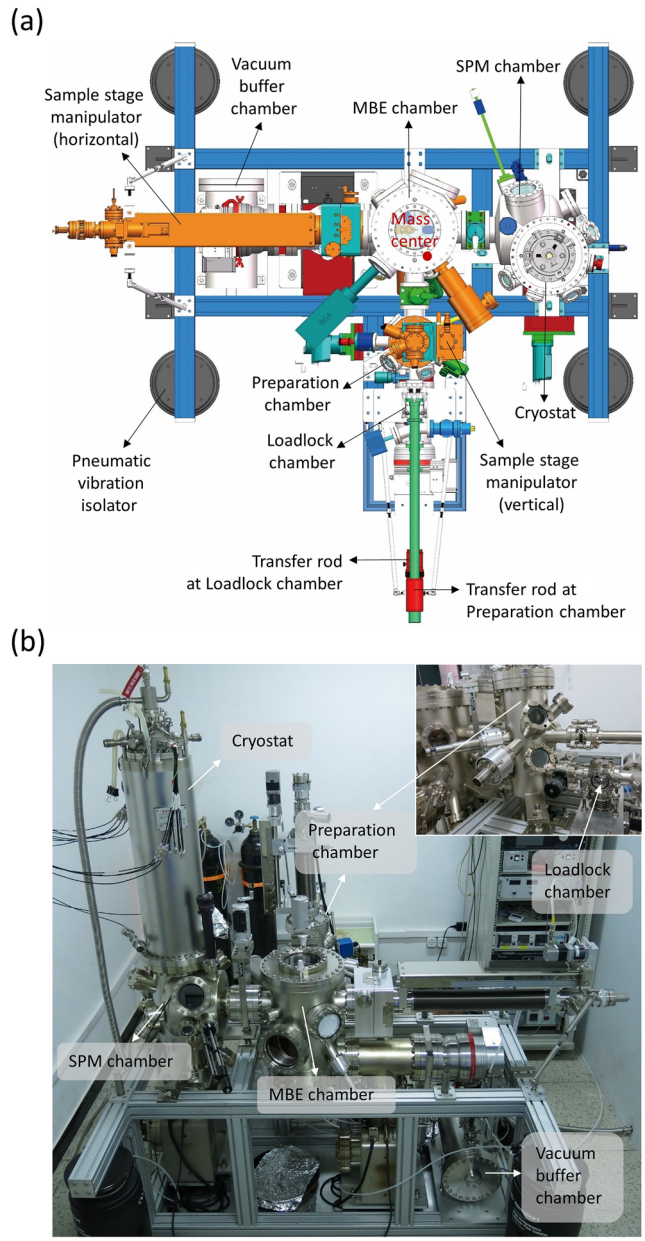

FIG. 1. 3D model and photograph of the system. (a) Top view of a 3D model of the system. (b) Photograph of the system. The preparation chamber and the load-lock chamber are shown in the inset.

aluminum beams (beam cross section size is 80 mm × 80 mm) supported by four pneumatic vibration isolators. The estimated mass center of the system is indicated by a red dot in Fig. 1(a). The system has four main chambers—an SPM chamber, an MBE chamber, a preparation chamber, and a load-lock chamber. A 700 l/s turbomolecular pump is installed on the MBE chamber and serves as the main pump for the system. The preparation chamber and the load-lock chamber share a 300 l/s turbomolecular pump. The outlet ports of both pumps are connected to a buffer chamber equipped with an 80 l/s turbomolecular pump. This design ensures a better vacuum level of the main chambers. The SPM chamber and the MBE chamber are both equipped with ion pumps of 300 l/s, and the preparation chamber is equipped with a smaller ion pump of 75 l/s. The internal volume of the load-lock chamber is only 195 ml, ensuring a short pump-down time from atmospheric pressure to high vacuum. Before baking, all the chambers and bakable parts of the system are enclosed in a tent made of thermal isolation materials. Two 5 kW heaters with fans are used to heat up the system to around 150 °C. Both the SPM chamber and the MBE chamber could reach below 5×10^{-11} Torr after one week's baking.

Samples and tips are mounted on a standard flag-style sample holder. Typically, the sample is loaded into the system from the load-lock chamber and then transferred to the sample stage of the manipulator vertically mounted on the preparation chamber by the transfer rod on the load-lock chamber. Cycles of ion bombardment and annealing (up to 1400 K) of the sample can be performed in the preparation chamber. After the cleaning process, the sample is transferred to the other manipulator, horizontally mounted on the MBE chamber, by the transfer rod on the preparation chamber. This two-transfer-rod design prevents direct connection between the load-lock chamber and the MBE chamber and thus helps maintaining a better vacuum inside the MBE chamber where the desired material is grown. After material growth, the sample is transferred to the SPM chamber by using the horizontal manipulator. Inside the SPM chamber, a wobble stick (CreaTec GmbH) is used to transfer the sample from the manipulator to the scanner head for cooling down and characterization. The SPM tip transfer follows the same path.

The MBE chamber, as shown in Fig. 2, can accommodate six evaporators simultaneously. As mentioned above, a horizontal manipulator is mounted on the chamber, on which the sample can be heated up to 1400 K by electron beam heating and cooled down to 120 K by continuous flow of liquid nitrogen. A cryo-shroud made of oxygen-free high-conductivity (OFHC) copper is installed inside the MBE chamber close to the inner wall and is attached to a small cryogen tank of ~2.3 l hung underneath the top flange of the chamber through two stainless steel pipes. This cryo-shroud works as a cryopump and helps improve the vacuum level. Moreover, a Reflection High-Energy Electron Diffraction (RHEED) system (electron

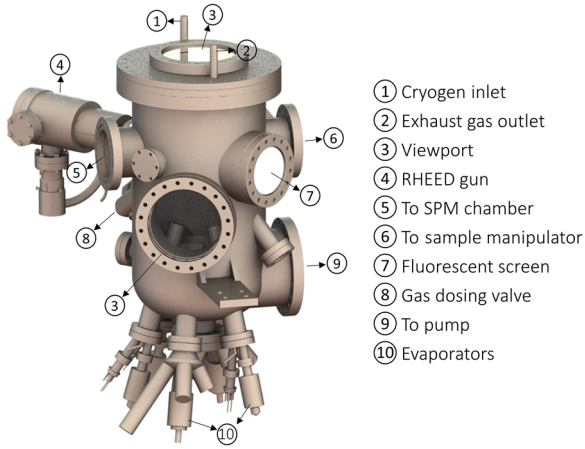

FIG. 2. 3D model of the MBE chamber. A sample manipulator is installed on the chamber through a DN100 ConFlat flange, indicated by No. 6 in the model. The MBE chamber connects to the SPM chamber though a port indicated by No. 5. The preparation chamber connects to a DN75 ConFlat flange at the rear side of this model.

energy ~ 15 keV) is installed for real-time monitoring of layered materials' growth. After the deposition of materials by MBE, the sample can be annealed *in situ* on the manipulator.

B. Cold room

A customized commercial cryostat from CryoVac GmbH is mounted on top of the SPM chamber, as indicated in Fig. 1(b). The volumes of the inner and outer cryogenic vessels are 4 l and 17 l for liquid helium (LHe) and liquid nitrogen (LN_2), respectively. A double-layer cold room, composed of a LN_2 shield and a LHe shield, is mounted at the bottom of the cryostat. The LN_2 shield has an octagonal frame with polished shielding sheets attached onto it, and the LHe shield has a similar structure but with a cuboid frame, as shown in Fig. 3(a). The frames and the shielding sheets are both made of aluminum alloy 6061. As has been demonstrated by plenty of tests by other laboratories and ourselves, aluminum alloy 6061 is ultrahigh vacuum (UHV) compatible. And it is also a good thermal conductor, ensuring efficient cooling of the shields. OFHC copper is another commonly used structure material in UHV environment and is an even better thermal conductor than aluminum alloy. However, aluminum alloy is much more lightweight than OFHC copper, making the assembling and mounting of the cold room a lot easier. Therefore, we chose aluminum alloy 6061 as the structure material of the cold room. Inside the LHe shield, the SPM scanner head is suspended by three mechanical springs made of Inconel alloy wire for vibration isolation. The calculated natural frequency of this suspension-spring system is around 1.56 Hz. Eight SmCo magnets are installed around the scanner head for vibration damping in both lateral and vertical directions. The combination of spring vibration isolation and magnetic damping proves to be efficient and is widely used in different kinds of SPM systems.[27–29]

Photo-assisted STM can provide a wealth of information of physical properties with atomic or molecular resolution. Quite a few approaches have been developed to build STMs with optical access paths.[30–33] In our system, the optical paths inside the SPM chamber are shown in Fig. 3(b). The angle of incidence is 50°. A pair of plane-convex fused silica lenses with 25.4 mm diameter is placed on both sides of the scanner head, located 60 mm away from the tunneling junction. We use a pair of piezo actuators, fastened to the LN_2 shield, to drive the movement of the lenses, as shown in Figs. 3(a) and 3(b). Each actuator is composed of three independent stepper positioners (attocube systems AG), and the lenses can move along three orthogonal directions with a travel range of 5 mm in each direction. Compared with some other designs that lenses are mounted on the chamber and driven by hand, several advantages are expected: (1) the thermal radiation to the tunneling junction is reduced because the lenses stay at LN_2 temperature; (2) fine and precise tuning of the lens position by piezo actuators improves the accuracy of light alignment; and (3) hands-free light alignment reduces disturbance in the data acquisition process. Besides, two pairs of windows are used to cover the optical openings on both LHe and LN_2 shields to further minimize the thermal radiation to the tunneling junction. Considering our potential application, the windows inside the vacuum and the viewports mounted on the SPM chamber along the optical path are all made of fused silica with transmission wavelengths from 200 nm to 2000 nm.

Since the LHe vessel in the cryostat is hung by a long tube, it is necessary to fix the LHe shield to the LN_2 shield during sample/tip transfer to the SPM scanner head. Clamping/unclamping of the LHe shield is achieved by rotating a clamping bolt using the wobble stick. The wobble stick is magnetically driven and thus is capable of conveying continuous rotary motions. During the clamping process, the movements of the related components, including a clamping bolt, a lever, a stainless steel belt, and a moving plate, are indicated by red arrows in Fig. 3(c). A magnetic damper is mounted under the LHe shield to dampen the lateral movements between the two shields. The magnets of this damper are glued to the moving plate. A 3D model of the complete cold room, including the shields, the optical components, the clamping structure, and the scanner head, is shown in Fig. 3(d).

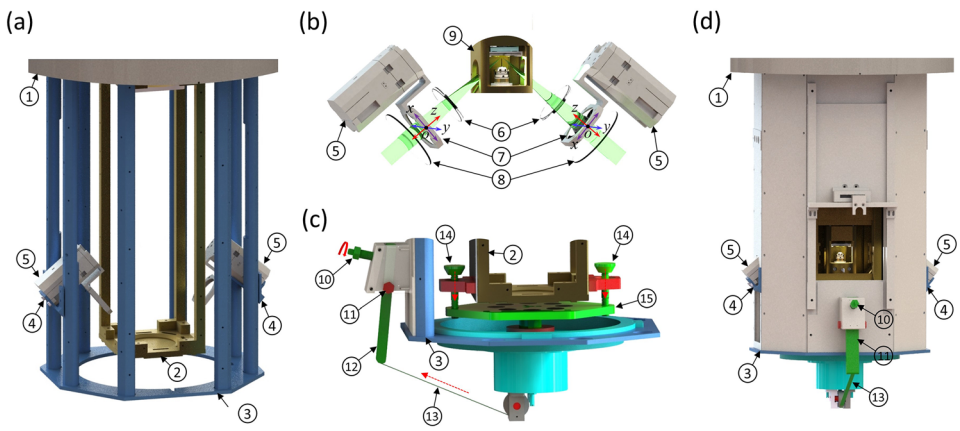

FIG. 3. Structure of the cold room. (a) The frames of the LHe shield (golden) and the LN_2 shield (blue). Two focus lenses are mounted on a pair of piezo-driven lens stages fastened on the LN_2 shield. (b) Optical components inside the cold room along the optical path, including two pairs of windows made of fused silica mounted on the LHe shield and LN_2 shield, and a pair of focus lenses. The moving directions of the lenses are indicated by the double-arrow axes marked as ox (purple), oy (blue), and oz (red) in the rectangular coordinates. (c) Clamping structure mounted at the bottom of the LN_2 frame to fix the LHe shield to the LN_2 shield. (d) The complete structure of the cold room with the SPM scanner head inside the LHe shield.

C. SPM scanner head

The scanner head is the most critical unit of an SPM system, as it largely determines the performance of the entire system. The Pan-type design,[34–36] due to its rigidity and reliability, proves to be one of the best designs for SPM scanner heads and is used in many systems.[28,37–39] Figure 4(a) shows the 3D model of our scanner head based on Pan's design. The scanner head is 31 mm × 31 mm × 79 mm in size and is composed of three main parts: the unibody frame, the tip-approach module, and the sample stage. This modular design makes it easy to assemble and maintain. Two optical openings are machined at both sides of the frame symmetrically for the access of light to the tunneling junction.

The tip-approach module has the classic structure of Pan's design: a customized piezo tube is glued coaxially to a sapphire prism shaft, and three pairs of shear piezo stacks drive the sapphire prism shaft in the slip-stick mode. A tip holder glued on top of the piezo tube is specially designed to accommodate both STM tips and qPlus sensors (CreaTec GmbH), providing additional flexibility for the system.[40] The vertical travel distance of the tip is 8 mm.

Tip-approach failure sometimes happens in Pan's stepper motor due to degradation of shear piezo stacks after long-term use or decreased sensitivity of piezo pieces at a low working temperature. One efficient way to address this issue is to adjust the friction between the shear piezo stacks and the prism shaft by changing the stress between them. In our design, we use one screw at the front side of the scanner head to complete the adjustment. By making the end of the stress-adjusting screw have a similar square handle as that of the sample plate, it is easy to use the wobble stick to twist it, making the *in situ* adjustment of the stress very easy under the UHV and LT condition.

In Pan's original design, the tip approach module is accommodated inside a C-shape frame with opening at one side covered by a spring plate. In our design, the tip-approach module is totally enclosed inside the frame. Finite element simulation is employed on the natural frequency analysis of these two different structures.[41] It shows that the base natural frequency of the enclosed design is higher, consistent with the intuitive knowledge.

The choice of the material for the scanner head is undoubtedly important and is a trade-off result. We chose titanium as the frame material taking into account of both the thermal compensation effect and the cooling efficiency. The thermal expansion coefficient of titanium is close to that of sapphire, which can minimize the strain generated due to the temperature effect. Macor (Corning, Inc.),[42] known as machinable glass-ceramic and used in original Pan's scanner head, is easier to be machined than titanium and its thermal expansion coefficient is also close to that of sapphire. However, the thermal conductivity of Macor is much lower than that of titanium.[42,43] Considering the cooling efficiency of the scanner head working in cryogenic temperature, titanium is a better choice for the frame.

The inertia piezoelectric motor (IPM) is a widely adopted technique to build nano-positioner systems.[44–46] A home-made coarse motion IPM is employed in the sample stage module to drive the sample's movement in X and Y directions, as shown in Fig. 4(b). The sample is fastened on a moving stage supported by three piezo stacks glued on it, each of which is composed of two piezo shear actuators (PI Ceramic GmbH), driving motions along two crossed directions, respectively. Driven by sawtooth wave voltage, similar to that of Pan's motor working in the slip-stick mode, the sample stage will move in a quasi-linear way along either direction based on the inertia piezoelectric mechanism. The traveling range is ±2.5 mm for

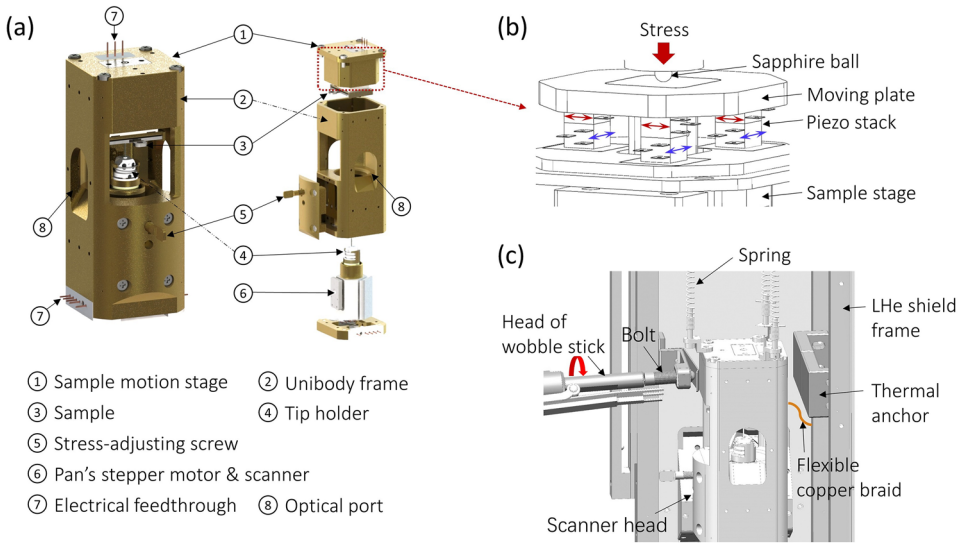

FIG. 4. Structure and cooling mechanism of the scanner head. (a) 3D model and exploded view of the scanner head. The stepper motor for tip-approach is based on Pan's design, with a travel distance of 8 mm. The sample is placed on a sample stage module with a moving range of 5 mm × 5 mm. Two optical openings are machined on both sides of the frame for optical access. (b) The structure of the IPM inside the sample stage. The moving directions of the piezo actuators are shown by red (X) and blue (Y) double arrows. The stress can be adjusted by a screw at the top of the sample stage. (c) The section view of the scanner head inside the LHe shield. The scanner head is levitated by three springs. One flexible copper braid, connecting the scanner head and the LHe shield frame, is used to increase the cooling efficiency. The scanner head can be clamped tightly against an OFHC copper thermal anchor mounted on the LHe shield frame by twisting a bolt shaft using the wobble stick.

each direction. The sample stage is mounted on top of the unibody frame. A silicon diode temperature sensor and a resistive heater are imbedded in the sample stage module.

For efficient cooling of the scanner head, one soft and flexible OFHC copper braid is used to connect the aluminum frame and the sample stage, as shown in Fig. 4(c). Moreover, each time before cooling, the scanner head will be pushed toward a thermal anchor made of OFHC copper mounted on the aluminum frame.[37,47] The scanner head can be clamped tightly against the thermal anchor for better cooling efficiency by twisting a bolt shaft using the wobble stick until they are in good thermal contact.

III. PERFORMANCE

To test the lowest working temperature of the scanner head, we covered the optical openings on the cold room with aluminum foils. When a sample at 300 K is transferred into the scanner head that stays at LHe temperature, the average cooling time is around 100 min. After cooling down, the temperature of the sample is around 5 K and lasts over 70 h. The frequency spectrum of the background current under 5 K with the tip retracted is shown in Fig. 5(a); the highest peak is below 8 fA/$\sqrt{\text{Hz}}$. The frequency spectrum of the tunneling current with feedback off is shown in Fig. 5(b), and the peaks are far below 1 pA/$\sqrt{\text{Hz}}$. These current frequency spectra indicate that the vibration isolation of the SPM is sufficient and the electrical grounding is effective. To demonstrate the stability of the SPM, we carried out a drift test at 5 K. The average lateral drift of the scanner head is 50 pm/h, which is tested by a continuous scanning of 12 h at a fixed area on an Au(111) sample with I_t = 300 pA, V_b = −1 V. The vertical drift of the scanner head is 35 pm/h, which was tested by continuously recording the tip position for 5 h with feedback on, under tunneling conditions with I_t = 500 pA, V_b = −1 V.

To demonstrate the spatial resolution as well as the imaging quality of our system, an electrochemically etched tungsten tip was used to scan a cleaned Au(111) substrate. The herringbone structure and atomic-resolution image of Au(111) were clearly resolved by STM, as shown in Figs. 6(a) and 6(b).

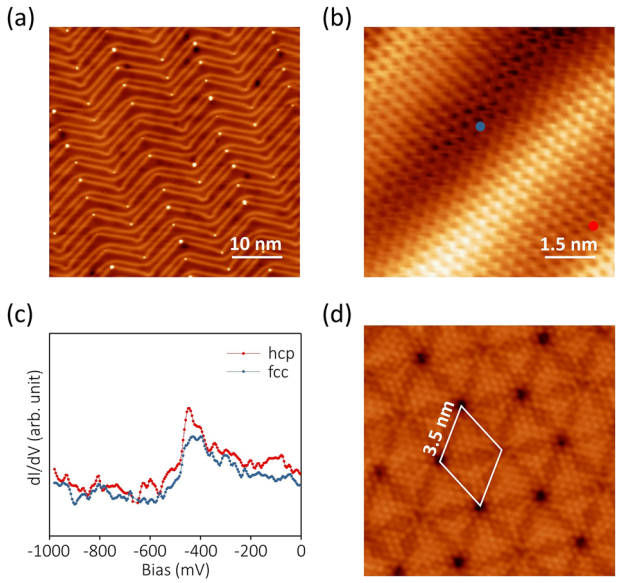

FIG. 6. STM characterization of the Au(111) surface and the Te-covered Au(111) surface. (a) Herringbone reconstruction of the Au(111) surface, I_t = 0.1 nA, V_b = −1 V. The bright dots at the elbows represent Te atoms. (b) Atomic resolution of the Au(111) surface. I_t = 0.5 nA, V_b = −1 V. (c) The *dI*/*dV* spectra at the fcc and hcp sites of the Au(111) surface. The hcp site is marked by a red dot and the fcc site is marked by a blue dot in (b). (d) Atomic resolution image of the hexagonal structure of the Te-covered Au(111) surface. I_t = 0.3 nA, V_b = −1 V.

In addition, scanning tunneling spectroscopy data were obtained on both the fcc and hcp sites, as shown in Fig. 6(c), consistent with the results reported by Chen *et al.*[48] During the acquisition of the *dI*/*dV* spectra, the tip was positioned at a fixed height with tunneling parameters of I_t = 1 nA, V_b = −500 mV. The amplitude and frequency of the modulation bias were 20 mV and 733 Hz, respectively.

To demonstrate the system's capability of *in situ* material growth and characterization, we deposited tellurium (Te) onto the Au(111) substrate by MBE. After annealing, we found that a periodic hexagonal lattice of Te atoms had formed. The atomic structure is clearly resolved by the STM, as shown in Fig. 6(d), with each bright spot representing a Te atom.

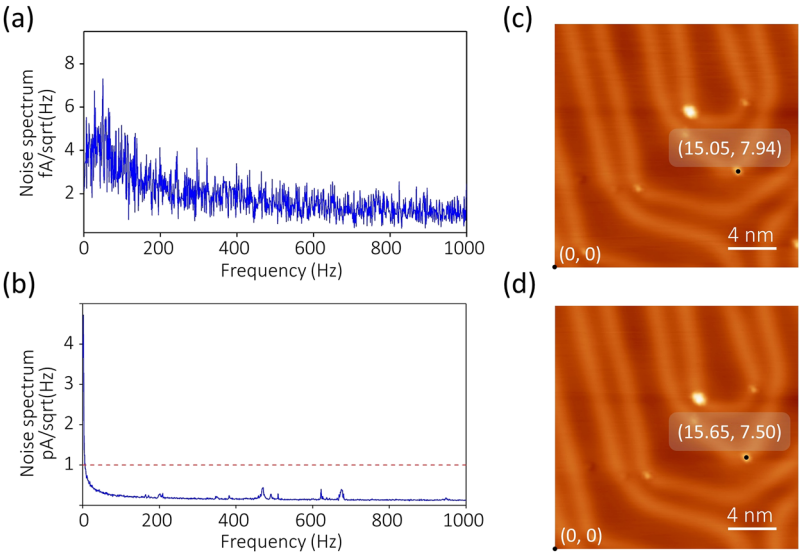

FIG. 5. Frequency spectra and drift test at a low temperature. (a) Frequency spectrum of the background current with the tip retracted. (b) Frequency spectrum of the tunneling current with the tip approached and feedback turned off. Before the acquisition of the spectra, the tip is positioned at a fixed height with I_t = −500 pA, V_b = −1 V. The bandwidth of the preamplifier is 4 kHz, and the feedback resistor is 10^9 Ω. [(c) and (d)] The first and the last STM images during the drift test with a time interval of 12 h. The black dot indicates an atomic cluster adsorbed at the elbow position on the Au(111) surface, the coordinate value of which is marked in both images. The left bottom corner marked by (0, 0) is set as the origin of the coordinate. The lateral drifts along different directions are not the same, which are 50 pm/h along the horizontal direction and 37 pm/h along the vertical direction.

The Te atoms are adsorbed onto the $\sqrt{3}$ sites of the Au(111) lattice. In each unit cell of this hexagonal structure, one triangular patch of half the Te atoms sits on the fcc sites, while the other patch sits on the hcp sites. The same structure has been prepared and reported by other groups recently.[49,50] The growth of the Te hexagonal structure on Au(111) using MBE, together with the clearly resolved atomic structures, demonstrates the capabilities of this system in both material growth and characterization.

IV. CONCLUSIONS

We report a UHV SPM system with MBE and optical access. The design of the system is presented and discussed. The SPM scanner head has a compact, rigid, and modular structure and can work in either STM mode or AFM mode. Forward compatibility to optical access into the STM tunneling junction is taken into consideration in the design of the scanner head, the cold room, and the SPM chamber. At the LHe temperature, the herringbone reconstruction feature, atomic resolution images, and dI/dV spectra of the Au(111) surface were obtained. The performance of the system is also demonstrated by the preparation and characterization of a periodic structure of Te on the Au(111) surface using MBE and STM. This system not only satisfies the basic requirements for material growth and characterization but is also highly compatible and stable.

ACKNOWLEDGMENTS

This work was supported by the National Major Scientific Instruments and Equipment Special Project (No. 2013YQ1203451) and the CAS Key Technology Research and Development Team Project. The authors thank Dr. Christoph Rüdt from CreaTec Fischer & Co. GmbH for his kind help in designing the tip holder.

[1] G. Binnig, H. Rohrer, C. Gerber, and E. Weibel, Phys. Rev. Lett. **49**, 57 (1982).
[2] G. Binnig, C. F. Quate, and C. Gerber, Phys. Rev. Lett. **56**, 930 (1986).
[3] C. J. Chen, *Introduction to Scanning Tunneling Microscopy* (Oxford University Press, 2008).
[4] E. Meyer, H. J. Hug, and R. Bennewitz, *Scanning Probe Microscopy: The Lab on a Tip* (Springer, Berlin, 2003).
[5] A. Y. Cho and J. R. Arthur, Prog. Solid State Chem. **10**, 157 (1975).
[6] A. A. Baker, W. Braun, G. Gassler, S. Rembold, A. Fischer, and T. Hesjedal, Rev. Sci. Instrum. **86**, 043901 (2015).
[7] Y. Zhang, K. He, C.-Z. Chang, C.-L. Song, L.-L. Wang, X. Chen, J.-F. Jia, Z. Fang, X. Dai, W.-Y. Shan, S.-Q. Shen, Q. Niu, X.-L. Qi, S.-C. Zhang, X.-C. Ma, and Q.-K. Xue, Nat. Phys. **6**, 584 (2010).
[8] L. Li, S.-Z. Lu, J. Pan, Z. Qin, Y.-Q. Wang, Y. Wang, G.-Y. Cao, S. Du, and H.-J. Gao, Adv. Mater. **26**, 4820 (2014).
[9] Y. Wang, L. Li, W. Yao, S. Song, J. T. Sun, J. Pan, X. Ren, C. Li, E. Okunishi, Y.-Q. Wang, E. Wang, Y. Shao, Y. Y. Zhang, H.-T. Yang, E. F. Schwier, H. Iwasawa, K. Shimada, M. Taniguchi, Z. Cheng, S. Zhou, S. Du, S. J. Pennycook, S. T. Pantelides, and H.-J. Gao, Nano Lett. **15**, 4013 (2015).
[10] X. Lin, J. C. Lu, Y. Shao, Y. Y. Zhang, X. Wu, J. B. Pan, L. Gao, S. Y. Zhu, K. Qian, Y. F. Zhang, D. L. Bao, L. F. Li, Y. Q. Wang, Z. L. Liu, J. T. Sun, T. Lei, C. Liu, J. O. Wang, K. Ibrahim, D. N. Leonard, W. Zhou, H. M. Guo, Y. L. Wang, S. X. Du, S. T. Pantelides, and H. J. Gao, Nat. Mater. **16**, 717 (2017).
[11] J. Lu, D.-L. Bao, K. Qian, S. Zhang, H. Chen, X. Lin, S.-X. Du, and H.-J. Gao, ACS Nano **11**, 1689 (2017).
[12] X. Wu, Y. Shao, H. Liu, Z. Feng, Y.-L. Wang, J.-T. Sun, C. Liu, J.-O. Wang, Z.-L. Liu, S.-Y. Zhu, Y.-Q. Wang, S.-X. Du, Y.-G. Shi, K. Ibrahim, and H.-J. Gao, Adv. Mater. **29**, 1605407 (2016).
[13] Y.-Q. Wang, X. Wu, Y.-L. Wang, Y. Shao, T. Lei, J.-O. Wang, S.-Y. Zhu, H. Guo, L.-X. Zhao, G.-F. Chen, S. Nie, H.-M. Weng, K. Ibrahim, X. Dai, Z. Fang, and H.-J. Gao, Adv. Mater. **28**, 5013 (2016).
[14] K. E. Aretouli, P. Tsipas, D. Tsoutsou, J. Marquez-Velasco, E. Xenogiannopoulou, S. A. Giamini, E. Vassalou, N. Kelaidis, and A. Dimoulas, Appl. Phys. Lett. **106**, 143105 (2015).
[15] Y. Terada, S. Yoshida, O. Takeuchi, and H. Shigekawa, Nat. Photonics **4**, 869 (2010).
[16] T. L. Cocker, V. Jelic, M. Gupta, S. J. Molesky, J. A. J. Burgess, G. D. L. Reyes, L. V. Titova, Y. Y. Tsui, M. R. Freeman, and F. A. Hegmann, Nat. Photonics **7**, 620 (2013).
[17] S. Li, S. Chen, J. Li, R. Wu, and W. Ho, Phys. Rev. Lett. **119**, 176002 (2017).
[18] P. Verma, Chem. Rev. **117**, 6447 (2017).
[19] J. Steidtner and B. Pettinger, Rev. Sci. Instrum. **78**, 103104 (2007).
[20] N. Jiang, E. T. Foley, J. M. Klingsporn, M. D. Sonntag, N. A. Valley, J. A. Dieringer, T. Seideman, G. C. Schatz, M. C. Hersam, and R. P. Van Duyne, Nano Lett. **12**, 5061 (2012).
[21] B. Pettinger, P. Schambach, C. J. Villagomez, and N. Scott, Annu. Rev. Phys. Chem. **63**, 379 (2012).
[22] E. A. Pozzi, G. Goubert, N. Chiang, N. Jiang, C. T. Chapman, M. O. McAnally, A.-I. Henry, T. Seideman, G. C. Schatz, M. C. Hersam, and R. P. V. Duyne, Chem. Rev. **117**, 4961 (2017).
[23] Y. Zhang, Y. Luo, Y. Zhang, Y.-J. Yu, Y.-M. Kuang, L. Zhang, Q.-S. Meng, Y. Luo, J.-L. Yang, Z.-C. Dong, and J. G. Hou, Nature **531**, 623 (2016).
[24] M. Lucas and E. Riedo, Rev. Sci. Instrum. **83**, 061101 (2012).
[25] R. Zhang, Y. Zhang, Z. C. Dong, S. Jiang, C. Zhang, L. G. Chen, L. Zhang, Y. Liao, J. Aizpurua, Y. Luo, J. L. Yang, and J. G. Hou, Nature **498**, 82 (2013).
[26] S. Grafström, J. Appl. Phys. **91**, 1717 (2002).
[27] R. Ma, Q. Huan, L. Wu, J. Yan, Q. Zou, A. Wang, C. A. Bobisch, L. Bao, and H.-J. Gao, Rev. Sci. Instrum. **88**, 063704 (2017).
[28] J. D. Hackley, D. A. Kislitsyn, D. K. Beaman, S. Ulrich, and G. V. Nazin, Rev. Sci. Instrum. **85**, 103704 (2014).
[29] B. C. Stipe, M. A. Rezaei, and W. Ho, Rev. Sci. Instrum. **70**, 137 (1999).
[30] K. Kuhnke, A. Kabakchiev, W. Stiepany, F. Zinser, R. Vogelgesang, and K. Kern, Rev. Sci. Instrum. **81**, 113102 (2010).
[31] N. J. Watkins, J. P. Long, Z. H. Kafafi, and A. J. Mäkinen, Rev. Sci. Instrum. **78**, 053707 (2007).
[32] J. G. Keizer, J. K. Garleff, and P. M. Koenraad, Rev. Sci. Instrum. **80**, 123704 (2009).
[33] S. Zhang, D. Huang, and S. Wu, Rev. Sci. Instrum. **87**, 063701 (2016).
[34] S. Pan, International Patent Publication Number WO 93/19494 (International Bureau, World Intellectual Property Organization, 30 September 1993).
[35] C. Wittneven, R. Dombrowski, S. H. Pan, and R. Wiesendanger, Rev. Sci. Instrum. **68**, 3806 (1997).
[36] S. H. Pan, E. W. Hudson, and J. C. Davis, Rev. Sci. Instrum. **70**, 1459 (1999).
[37] S. Misra, B. B. Zhou, I. K. Drozdov, J. Seo, L. Urban, A. Gyenis, S. C. J. Kingsley, H. Jones, and A. Yazdani, Rev. Sci. Instrum. **84**, 103903 (2013).
[38] Y. J. Song, A. F. Otte, V. Shvarts, Z. Zhao, Y. Kuk, S. R. Blankenship, A. Band, F. M. Hess, and J. A. Stroscio, Rev. Sci. Instrum. **81**, 121101 (2010).
[39] J. Kim, H. Nam, S. Qin, S.-U. Kim, A. Schroeder, D. Eom, and C.-K. Shih, Rev. Sci. Instrum. **86**, 093707 (2015).
[40] A. M. Lakhani, S. J. Kelly, and T. P. Pearl, Rev. Sci. Instrum. **77**, 043709 (2006).
[41] S. C. White, U. R. Singh, and P. Wahl, Rev. Sci. Instrum. **82**, 113708 (2011).
[42] See https://www.corning.com/au/en/products/advanced-optics/product-materials/specialty-glass-and-glass-ceramics/glass-ceramics/macor.html for Corning Incorporated.
[43] R. W. Powell and R. P. Tye, J. Less Common Met. **3**, 226 (1961).
[44] W. Ge, J. Wang, J. Wang, J. Zhang, Y. Hou, and Q. Lu, Rev. Sci. Instrum. **88**, 126102 (2017).
[45] L. Liu, W. Ge, W. Meng, Y. Hou, J. Zhang, and Q. Lu, Rev. Sci. Instrum. **89**, 033704 (2018).

[46]J. Wang and Q. Lu, Rev. Sci. Instrum. **83**, 093701 (2012).
[47]U. R. Singh, M. Enayat, S. C. White, and P. Wahl, Rev. Sci. Instrum. **84**, 013708 (2013).
[48]W. Chen, V. Madhavan, T. Jamneala, and M. F. Crommie, Phys. Rev. Lett. **80**, 1469 (1998).
[49]J. Guan, X. Huang, X. Xu, S. Zhang, X. Jia, X. Zhu, W. Wang, and J. Guo, Surf. Sci. **669**, 198 (2018).
[50]C. Gu, S. Zhao, J. L. Zhang, S. Sun, K. Yuan, Z. Hu, C. Han, Z. Ma, L. Wang, F. Huo, W. Huang, Z. Li, and W. Chen, ACS Nano **11**, 4943 (2017).